A Triangular Iron(III) Complex Potentially Relevant to Iron(III)-Binding Sites in Ferreascidin

Eckhard Bill, Carsten Krebs, Manuela Winter, Michael Gerdan, Alfred X. Trautwein, Ulrich Flörke, Hans-Jürgen Haupt, and Phalguni Chaudhuri*

Abstract: An asymmetric triangular Fe^{III} complex has been synthesized by an unusual Fe^{II}-promoted activation of salicylaldoxime. Formation of the ligand 2-(bis(salicylideneamino)methyl)phenol in situ is believed to occur through the reductive deoximation of salicylaldoxime by ferrous ions. The trinuclear ferric complex has been characterized on the basis of elemental analysis, IR, variable-temperature magnetic susceptibility, and EPR and Mössbauer spectroscopies. The molecular structure established by X-ray diffraction consists of a trinuclear structure with a $[Fe_3(\mu_3\text{-}O)(\mu_2\text{-}OPh)]^{6+}$ core. Two iron ions are in a distorted octahedral environment having FeN_2O_4 coordination spheres, and the five-coordinated third iron ion, with an $FeNO_4$ coordination sphere, is in a trigonal bipyramidal environment. The magnetic susceptibility measurements revealed an $S_t = 5/2$ ground state with the antiparallel exchange interactions $J = -34.3\ cm^{-1}$, $J' = -4.7\ cm^{-1}$, and $D = -0.90\ cm^{-1}$. The EPR results are consistent with a ground state of $S = 5/2$ together with a negative $D_{5/2}$ value. The Mössbauer isomer shifts together with the quadrupole splitting also provide evidence for the high-spin state of the three ferric sites. Magnetic Mössbauer spectra lead to the conclusion that the internal magnetic fields possibly lie in the plane of the three ferric ions.

Keywords
EPR spectroscopy · exchange coupling · iron · Moessbauer spectroscopy · O ligands

Introduction

The current interest in the chemistry of polynuclear systems with two or more Fe^{III} ions bridged by oxygen-donor ligands is mainly due to the growing awareness of the existence of oxo-bridged iron units in a variety of iron metalloproteins.[1] The pursuit of model complexes for the iron proteins has yielded several interesting polynuclear ferric complexes with unusual electronic structures.[2]

The stability of its metal complexes lies behind the diverse applications of salicylaldoxime and its various substituted derivatives, from analytical reagents to extractants in hydrometallurgy and as corrosion inhibitors.[3] It has been reported that the oxime functionality can be chemically activated by binding to a metal center such as VO^{2+} or Pt^{IV}.[4] We report here a trinuclear Fe^{III} compound obtained by an unusual Fe^{II}-promoted activation of salicylaldoxime.

Ferreascidin,[5] a glycoprotein with a molecular weight of 10 kDa, is isolated from the blood cells of the stolidobranch ascidian (*Pyura stolonifera*). Ferreascidin as isolated does not contain any metal ions; the protein derives its name from its strong iron-binding ability, with an effective stability constant of $4 \times 10^{17}\ M^{-1}$ at pH 7.0. The most characteristic feature of this protein is its content of aromatic amino acids (42% tyrosine, 17% (3,4-dihydroxyphenyl)alanine (DOPA), 8% phenylalanine), by far the highest described to date for any natural protein. It is also remarkable that ferreascidin contains the "non-protein" amino acid DOPA. Recently, EPR and Mössbauer spectroscopic investigation of the interaction of iron(III) with ferreascidin revealed the existence of at least three distinct iron(III)-binding sites.[6] One of the sites (site 3) is the first example of a trinuclear iron(III) cluster as a metal-binding domain in a metalloprotein. The authors favored a linear trinuclear Fe^{III} cluster as the structure for the metal-ion-binding site 3, on the basis of its paramagnetic ground state with $S = 5/2$. μ-Oxo, μ-hydroxo and μ-phenoxo groups have been considered as candidates for the bridging ligands, although no unequivocal identification of the bridging ligands present at site 3 could be made. The triangular μ_3-oxo bridged Fe^{III} structural motif present in the "basic carboxylates" of Fe^{III} has been eliminated, because the lowest spin state of the known trinuclear carboxylates is $S = 1/2$, which is inconsistent with the $S = 5/2$ ground state of the protein. Although the molecular mass of the

[*] P. Chaudhuri, E. Bill, C. Krebs, M. Winter
Max-Planck-Institut für Strahlenchemie
P. O. Box 101365, D-45413 Mülheim an der Ruhr (Germany)
e-mail: chaudh@mpi-muelheim.mpg.de
M. Gerdan, A. X. Trautwein
Institut für Physik, Medizinische Universität, D-23538 Lübeck (Germany)
U. Flörke, H.-J. Haupt
Anorganische und Analytische Chemie
Universität-Gesamthochschule Paderborn, D-33098 Paderborn (Germany)

protein is quite small, the microheterogeneity of the protein eliminates the possibility of structural determination by X-ray crystallography. Hence the model complex approach appears to present the best opportunity to investigate the iron(III)-binding sites in ferreascidin further.

With the above-mentioned points in mind, we describe here the synthesis of an asymmetric triangular iron(III) complex by the reductive cleavage of salicylaldoxime with iron(II) chloride and its characterization by X-ray diffractometry, susceptibility measurements, and EPR and Mössbauer spectroscopy.

Experimental Section

The starting materials were commercially available and used as received. Elemental analyses (C, H, N) were performed by the Microanalytical Laboratory, Ruhr-Universität Bochum. Iron was determined spectrophotometrically as its pyridine-2,6-dicarboxylic acid complex. Electronic absorption spectra were measured on a Perkin–Elmer Lambda 9 spectrophotometer in an acetonitrile solution. Fourier-transform infrared spectroscopy (KBr pellets) was performed on a Perkin–Elmer 1720X FT-IR instrument. Magnetic susceptibilities of the polycrystalline sample were recorded on a SQUID magnetometer (MPMS, Quantum Design) in the temperature range 5.3–300 K with an applied field of 1 T. Experimental susceptibility data were corrected for underlying diamagnetism with Pascal's constants ($\chi_{Dia} = 533 \times 10^{-6}$ cm^3 mol^{-1}). A Bruker ESP 300 E X-band spectrometer with Bruker dual mode cavity in perpendicular mode and an Oxford ESR 910 helium-flow cryostat were used for the EPR experiments. The thermostat was calibrated against temperature measurements with a standard [7]. Mössbauer data were recorded on alternating constant-acceleration spectrometers. The minimum experimental linewidth was 0.24 mm s^{-1} full width at half maximum. The sample temperature was kept constant either in an Oxford Variox or an Oxford Mössbauer-Spectromag cryostat. The latter is a split-pair superconducting magnet system for applying fields up to 8 T to the samples, which can be kept at temperatures in the range 1.5 K to 250 K. The field at the sample is perpendicular to the γ-beam. With the help of reentrant bore tubes the ^{57}Co/Rh source was positioned at room temperature inside the gap of the magnet system at a distance of about 85 mm from the sample. The field is zero at this position. Isomer shifts are given relative to α-Fe at room temperature.

Synthesis of $[(C_2H_5)_3NH][Fe_3(O)(C_{21}H_{15}N_2O_3)(C_7H_5NO_2)_2(C_7H_6NO_2)]\cdot 2H_2O$ (1): A methanolic solution (50 mL) of salicylaldoxime ($C_7H_7NO_2$, 0.72 g, 6 mmol) and triethylamine (1.5 mL) was purged with argon for 10 min before the solution was charged with a solid sample of $FeCl_2\cdot 4H_2O$ (0.4 g, 2 mmol). The resulting blue solution turned deep brown on stirring for 10 min and the stirring was continued for a further 2 h. The dark solution was filtered in air to remove any solid particles and the filtrate was kept at ambient temperature. After 2 d red-brown crystals were collected by filtration and air-dried. Yield: 0.17 g (10%); anal. calcd for $C_{48}H_{51}N_6O_{12}Fe_3$: C 53.81, H 4.80, N 7.84, Fe 15.63; found: C 53.8, H 4.8, N 7.7, Fe 15.5; IR spectral data (KBr pellets): 3045 (w), 1617 (s), 1597 (s), 1542 (s), 1472 (s), 1440 (s), 1420 (s), 1293 (s), 1266 (s), 1197 (m), 1151 (m), 1124 (w), 1017 (m), 912 (s), 814 (m), 755 (m), 665 (m), 608 (m), 566 (m), 436 (m) cm^{-1}; UV/VIS in CH_3CN: λ (ε) = 409 (16718), $\approx$300 sh (39215), 225 (101699) nm (L mol^{-1} cm^{-1}).

Crystal structure determination: The diffraction intensities of a red-brown crystal of **1** with dimensions 0.12 × 0.15 × 0.60 mm were collected by means of a Siemens R3m/V diffractometer with graphite-monochromated $Mo_{K\alpha}$ radiation at 293 ± 1 K and the ω–2θ scan technique with a θ range of 2.36 to 27.56°. A total of 12085 reflections were collected in the index ranges $-11 \le h \le 11$, $0 \le k \le 33$, $0 \le l \le 28$, of which 11796 were unique and 2236 were considered significant with $F > 4\sigma(F)$. Preliminary examination showed that the crystal belonged to the monoclinic crystal system, space group $P2_1/n$. The lattice parameters were obtained by a least-squares refinement of the angular settings ($15 \le 2\theta \le 30°$) of 30 reflections. Pertinent crystallographic data are summarized in Table 1. The data were corrected for Lorentz and polarization effects, but it was not necessary to account for crystal decay. An empirical absorption correction by ψ scans was carried out. The scattering factors for neutral non-hydrogen atoms were corrected for both the real and the imaginary components of anomalous dispersion. The structure was determined by direct methods (SHELXTL-PLUS). The final cycle of full-matrix least-squares refinement on F^2 was based on all 11796 reflections and 586 variable parameters and converged with agreement factors of $R1 = 0.0893$ [$F > 4\sigma(F)$] and $wR2 = 0.321$ (all data) (SHELXL-93). All non-hydrogen atoms were refined anisotropically; isotropic H atoms were fixed in idealized positions (riding model). One ethyl group of the triethylammonium cation was disordered over two sites with site occupation factors 0.41 and 0.59. The maximum and minimum peaks on the final difference Fourier map correspond to 1.158 and -0.994 e Å^{-3}, respectively. Selected interatomic distances and angles are given in Table 2.

Table 1. Summary of crystallographic data for $[(C_2H_5)_3NH][C_{42}H_{31}Fe_3N_5O_{10}]\cdot 2H_2O$ (**1**).

formula	$C_{48}H_{51}N_6O_{12}Fe_3$
M_r	1071.52
space group	$P2_1/n$
a (Å)	9.136(2)
b (Å)	25.845(8)
c (Å)	21.628(9)
β (°)	90.89(2)
V (Å^3)	5106(3)
ρ_c (g cm^{-3})	1.398
Z	4
μ (mm^{-1})	0.91
λ (Å)	0.71073
T (K)	293(1)
$R1$ [a]	0.0893
$wR2$ [b]	0.3212

[a] $R1 = \sum||F_o| - |F_c||/\sum|F_o|$. [b] $wR2 = [\sum[w(F_o^2 - F_c^2)^2]/\sum[w(F_o^2)^2]]^{\frac{1}{2}}$.

Table 2. Selected bond lengths (Å) and angles (°) for **1**.

Fe(1)–O(11)	1.949(6)	Fe(1)–O(12)	1.954(6)
Fe(1)–O(1)	1.982(5)	Fe(1)–O(2)	2.062(5)
Fe(1)–N(11)	2.125(7)	Fe(1)–N(12)	2.130(6)
Fe(2)–O(22)	1.934(6)	Fe(2)–O(21)	1.966(6)
Fe(2)–O(1)	1.968(5)	Fe(2)–O(2)	2.090(5)
Fe(2)–N(21)	2.132(6)	Fe(2)–N(22)	2.143(6)
Fe(3)–O(1)	1.917(5)	Fe(3)–O(31)	1.920(5)
Fe(3)–O(4)	1.935(6)	Fe(3)–O(3)	1.951(6)
Fe(3)–N(31)	2.098(8)		
O(3)–N(11)	1.370(8)	O(4)–N(21)	1.357(8)
O(32)–N(31)	1.413(9)	N(11)–C(1)	1.311(10)
N(12)–C(8)	1.302(10)	N(12)–C(36)	1.492(9)
N(21)–C(15)	1.283(10)	N(22)–C(22)	1.272(9)
N(22)–C(36)	1.491(9)	N(31)–C(29)	1.280(11)
C(36)–C(37)	1.491(11)		
O(11)-Fe(1)-O(12)	96.8(3)	O(11)-Fe(1)-O(1)	163.3(2)
O(12)-Fe(1)-O(1)	96.7(2)	O(11)-Fe(1)-O(2)	88.9(2)
O(12)-Fe(1)-O(2)	169.6(2)	O(1)-Fe(1)-O(2)	79.3(2)
O(11)-Fe(1)-N(11)	84.3(3)	O(12)-Fe(1)-N(11)	95.1(2)
O(1)-Fe(1)-N(11)	84.8(2)	O(2)-Fe(1)-N(11)	94.2(2)
O(11)-Fe(1)-N(12)	94.1(2)	O(12)-Fe(1)-N(12)	86.4(2)
O(1)-Fe(1)-N(12)	96.6(2)	O(2)-Fe(1)-N(12)	84.6(2)
N(11)-Fe(1)-N(12)	177.9(3)	O(22)-Fe(2)-O(21)	96.9(3)
O(22)-Fe(2)-O(1)	99.1(2)	O(21)-Fe(2)-O(1)	161.0(2)
O(22)-Fe(2)-O(2)	169.0(2)	O(21)-Fe(2)-O(2)	87.2(2)
O(1)-Fe(2)-O(2)	79.0(2)	O(22)-Fe(2)-N(21)	94.6(2)
O(21)-Fe(2)-N(21)	84.3(2)	O(1)-Fe(2)-N(21)	84.2(2)
O(2)-Fe(2)-N(21)	95.9(2)	O(22)-Fe(2)-N(22)	85.8(2)
O(21)-Fe(2)-N(22)	93.2(2)	O(1)-Fe(2)-N(22)	98.2(2)
O(2)-Fe(2)-N(22)	83.8(2)	N(21)-Fe(2)-N(22)	177.5(2)
O(1)-Fe(3)-O(31)	170.1(2)	O(1)-Fe(3)-O(4)	93.8(2)
O(31)-Fe(3)-O(4)	92.4(2)	O(1)-Fe(3)-O(3)	94.7(2)
O(31)-Fe(3)-O(3)	90.4(2)	O(4)-Fe(3)-O(3)	110.0(3)
O(1)-Fe(3)-N(31)	85.9(2)	O(31)-Fe(3)-N(31)	84.3(3)
O(4)-Fe(3)-N(31)	123.0(3)	O(3)-Fe(3)-N(31)	126.8(3)
Fe(3)-O(1)-Fe(2)	119.0(2)	Fe(3)-O(1)-Fe(1)	118.0(2)
Fe(2)-O(1)-Fe(1)	101.8(2)		

0947-6539/97/0302-0194 $ 15.00+.25/0 Chem. Eur. J. 1997, 3, No. 2

Crystallographic data (excluding structure factors) for the structure reported in this paper have been deposited with the Cambridge Crystallographic Data Centre as supplementary publication no. CCDC-1220-46. Copies of the data can be obtained free of charge on application to the Director, CCDC, 12 Union Road, Cambridge CB2 1EZ, UK (Fax: Int. code + (1223) 336-033; e-mail: teched@chemcrys.cam.ac.uk).

Results and Discussion

The trinuclear Fe^{III} compound **1** has been obtained by an unusual Fe^{II}-promoted activation of salicylaldoxime. The in-situ formation of the ligand H_3salmp [2-(bis(salicylideneamino)-methyl)phenol] from the starting salicylaldoxime is believed to occur by the reaction pathway shown in Scheme 1. The use of

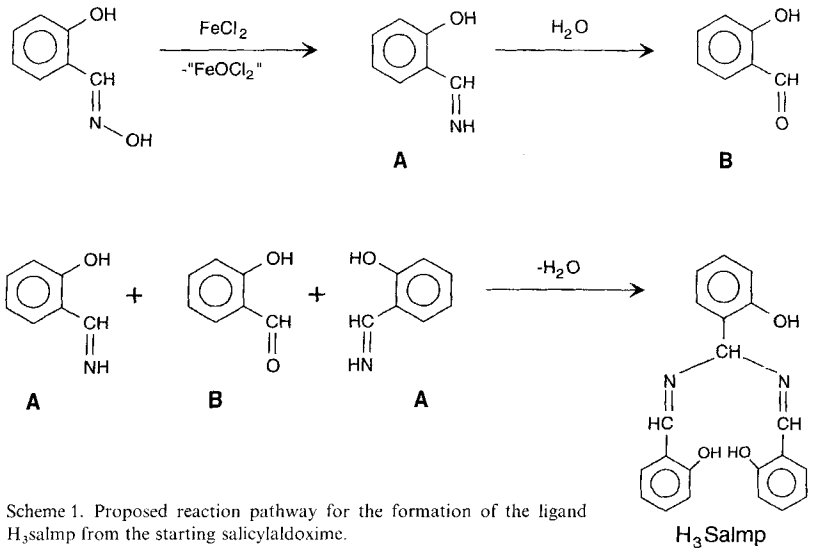

Scheme 1. Proposed reaction pathway for the formation of the ligand H_3salmp from the starting salicylaldoxime.

transition-metal ions with strong reducing properties, such as Cr^{II}, Ti^{II}, Ti^{III}, V^{II}, etc., has been reported by Olah and co-workers for the reductive deoximation of oximes to carbonyl compounds.[8]

The IR spectrum of **1** exhibits two strong sharp bands at 1616 and 1597 cm^{-1}, which can be ascribed to the $\tilde{\nu}$(CN) vibrations, whereas the medium intensity band at 1151 cm^{-1} is assignable to the NO stretching vibration. It is worth noting that **1** exhibits two sharp bands of medium intensity at 608 and 566 cm^{-1} from the Fe–O stretching vibrations.

Description of the structure: Although the analytical and spectroscopic data unambiguously showed the presence of a trinuclear Fe_3O core as the smallest unit in the anion, an X-ray analysis was undertaken to remove the doubts regarding connectivity. Unfortunately, crystals of the anion as its triethylammonium salt diffract X-rays very weakly. Nevertheless after several attempts we were able to collect a set of diffraction data of mediocre quality. In spite of the high R factor and large standard deviation resulting from the limited data from a weakly diffracting crystal, the crystal structure analysis of **1** confirmed its novel trinuclear structure with the $[Fe_3(\mu_3\text{-}O)(\mu_2\text{-}OPh)]^{6+}$ core. The entire structure of the anion in **1** is shown in Figure 1, while Figure 2 highlights the coordination spheres of the three iron atoms. The anion possesses an asymmetric

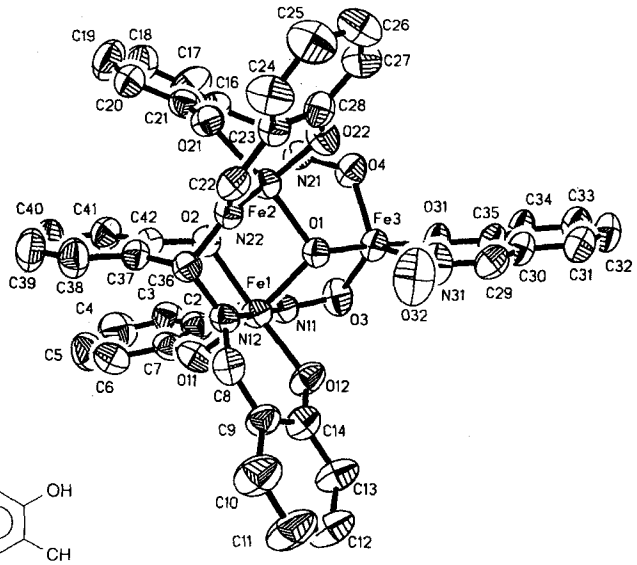

Figure 1. Structure of the trinuclear anion in **1**, showing the atom numbering scheme.

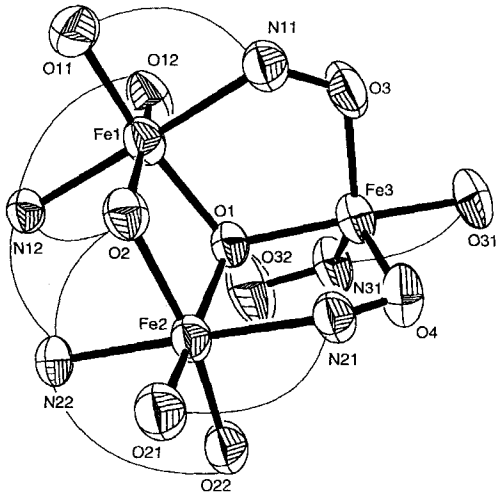

Figure 2. Structure of the iron coordination spheres in **1**.

$Fe_3(\mu_3\text{-}O)(\mu_2\text{-}O)$ core. The Fe(2)···Fe(1) distance, 3.065(1) Å, is noticeably shorter than the Fe(2)···Fe(3) and Fe(1)···Fe(3) distances, 3.348(1) and 3.342(1) Å, respectively. The disposition of the μ_3-oxide O(1) is not symmetrical, the differences being significant, Fe(1)–O(1) 1.982(5) Å, Fe(2)–O(1) 1.968(5) Å, and Fe(3)–O(1) 1.917(5) Å.

The iron ions Fe(1) and Fe(2) are in distorted octahedral environments, having FeN_2O_4 coordination spheres, and Fe(3) is in a trigonal bipyramidal $FeNO_4$ environment. Fe(1) is coordinated to N(12) and O(12) of the salmp^{3-} [2-(bis(salicylideneamino)methyl)phenolate] ligand, to O(11) and N(11) of a salicylaldoxime ligand, to the doubly bridging phenolate oxygen, O(2), and the triply bridging μ_3-O(1), thus yielding six-coordination at Fe(1). The atom connectivities for Fe(2) are very similar. The bridging Fe(1)–O(2) 2.062(5) Å, Fe(2)–O(2) 2.090(5) Å, and Fe(1)···Fe(2) 3.065(1) Å distances in **1** are very close to those of the binuclear species with the ligand H_3salmp, $[Fe_2(salmp)_2]$.[9] Fe(3) is coordinated to μ_3-O(1), to O(3) and O(4) of the deprotonated hydroxy groups of two neighboring

salicylaldoxime ligands, and to O(31) and N(31) of the third salicylaldoxime. The single negative charge of the anion in **1** leads us to conclude that the oxygen O(32) of the hydroxy group in the salicylaldoxime bonded only to Fe(3) is protonated. Accordingly the average N–O bond lengths in the N-O-Fe units are somewhat shorter, 1.364(7) Å, than the N(31)-O(32) distance of 1.413(9) Å. The distance Fe(3)···O(32), 2.993(7) Å, is long for bond formation. Thus a five-coordinated Fe^{III}, Fe(3), with a trigonal bipyramidal geometry prevails in **1**. The $FeNO_4$ coordination sphere is rare for trivalent iron with O,N-based ligation; octahedral coordination is by far the most common for Fe^{III}.[10] The Fe–N and Fe–O bond distances are consistent with a d^5 high-spin electron configuration of the Fe^{III} centers with azomethine nitrogen and phenolate oxygen-donor ligands.[9,11]

The three iron ions define an isosceles triangle, and the μ_3-oxo atom O(1) is displaced from the metal planes by 0.52(1) Å, further than in similar $Fe_3(\mu_3\text{-O})$ compounds ($\approx$0.24 Å). The average Fe–(μ_3-O) bond distance of 1.96 Å is noticeably longer than that observed for typical $Fe_3(\mu_3\text{-O})$ species, 1.90 Å.[12]

Magnetic susceptibility measurements: Magnetic susceptibility data for a polycrystalline sample of **1** were collected in the temperature range 5–300 K; the data are displayed in Figure 3 as

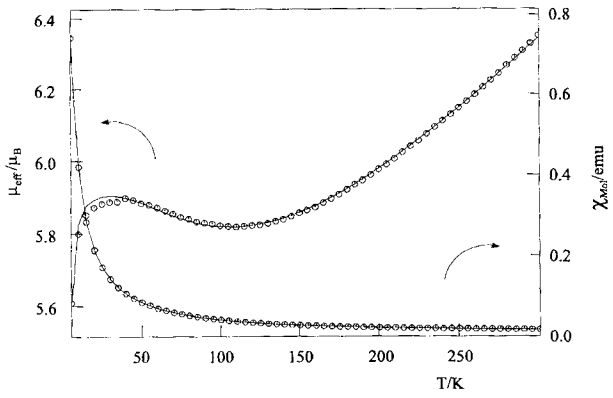

Figure 3. Plot of the experimental and calculated (solid lines) μ_{eff} and χ_M of **1** as a function of temperature.

μ_{eff} and χ_M vs. temperature. At 300.3 K the μ_{eff} value of 6.355 μ_B ($\chi_M \times T = 5.05\ cm^3\,mol^{-1}\,K$) is much lower than the value of $\mu_{eff} = 10.254\ \mu_B$ expected for three uncoupled spins of $S = 5/2$ with an average $g = 2.00$. On lowering the temperature, μ_{eff} decreases monotonically, approaching a broad minimum around 100–115 K, and increases upon further cooling. The temperature behavior of the magnetic susceptibility of **1** clearly indicates an antiferromagnetic coupling between the $S = 5/2$ of high-spin Fe^{III} centres. μ_{eff} reaches a maximum with a value of 5.90 μ_B ($\chi_M \times T = 4.352\ cm^3\,mol^{-1}\,K$) at 40 K, which is very close to the value of 5.92 μ_B for a hypothetically isolated $S = 5/2$. An $S = 5/2$ state is expected as the ground state for an antiferromagnetically coupled isosceles trinuclear Fe^{III} complex. Below 40 K there is a decrease in μ_{eff} for **1**, which reaches a value of 5.61 μ_B at 5.3 K; this behavior might be attributed to the splitting in the zero field of the ground state.

The experimental magnetic data were simulated by a least-squares-fitting computer program with a full-matrix diagonalization approach including exchange coupling, Zeeman splitting, and single-ion zero-field splitting. After diagonalization the energies (E_i) and magnetic moments [$\delta(E_i)/\delta(B)$] of each state were used to calculate the molar paramagnetic susceptibility as a function of temperature. The Hamiltonian in use to describe paramagnetism is given in Equation (1), where spin

$$\mathcal{H} = -2J_{ik}\boldsymbol{S}_i\boldsymbol{S}_k + \sum_{i=1}^{3} g_i\mu_B\boldsymbol{B}\boldsymbol{S}_i + D_i[S_{zi}^2 - \tfrac{1}{3}S(S+1) + E/D_i(S_{xi}^2 - S_{yi}^2)] \quad (1)$$

S_i is 5/2 and D_i is the axial zero-field splitting parameter. The term E/D_i measures the rhombic distortions. The presence of rhombicity has been observed from a preliminary EPR measurement of **1**. From rhombograms for an $S = 5/2$ spin state a value for $|E/D| = 0.3$ was obtained; hence we have kept $E/D_i = 0.33$ fixed during the fitting procedure of magnetic data. The Zeeman interaction of the high-spin ferric ion in the $^6A_1$ ground state with practically no contribution from the orbital angular momentum is isotropic and the observed g_{Fe} values are very close to the free-electron spin value of 2.00. Hence we have fixed g_i at 2.0.

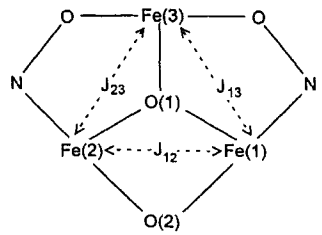

Scheme 2. Exchange coupling model for **1**.

The exchange coupling model is shown in Scheme 2. In this model J_{ik} represents the exchange interaction between the *i*th and *k*th paramagnetic iron(III) ions; as the trinuclear iron(III) framework forms an isosceles triangle, $J_{23} = J_{13} = J$ describes the interaction of Fe(3) with Fe(2) and Fe(1), $J_{12} = J'$ the interaction between the Fe(2) and Fe(1) ions.

Additionally, Mössbauer spectroscopy provides strong support for the high-spin, ferric, nature of iron in **1**; isomer shifts and quadrupole splittings were observed for the three iron sites, which are characteristic for $S = 5/2$ iron with ligand coordination as in Figure 1.

At the beginning we intuitively assumed that **1** owes its $S = 5/2$ ground state to a strong antiferromagnetic coupling J_{12}, which enforces "spin-pairing" of Fe(1) and Fe(2) and dominates the antiferromagnetic coupling constants J_{13} and J_{23} with Fe(3). This appeared plausible as besides superexchange through the μ_3-oxo group the coupling of Fe(1) and Fe(2) can also be mediated by the μ_2-phenoxo bridge, whereas the pathway to Fe(3) would be by the longer oxime -N–O- bonds. This presumption is augmented by the fact that the iron centres in the binuclear [$LFe^{III}Fe^{III}(SaO)_3$] complex (L = 1,4,7-trimethyl-1,4,7-triazacyclononane) is weakly antiferromagnetically coupled, with a coupling constant of $J = -12.5\ cm^{-1}$, the mediators being three salicylaldoximate(2–) (SaO) bridging groups.[11b,13] A spin-Hamiltonian fit starting with $|J'| > |J|$ yielded a good fit with $J' = -366.0\ cm^{-1}$ and $J = -5.0\ cm^{-1}$. The unusually large J', unprecedented in iron–oxo chemistry, led us to perform a systematic search in parameter space to determine the nature of the fit minimum.

0947-6539/97/0302-0196 $ 15.00+.25/0 Chem. Eur. J. 1997, 3, No. 2

A three-dimensional view of the relative error surface and best-fit contours for fitting the magnetic data of the complex as a function of both J and J' is shown in Figure 4. The error map in fact reveals the existence of a second minimum, which is a well-defined global minimum in the parameter space at $|J'| < |J|$. The correspondingly calculated (Figure 3, solid lines) χ_M and μ_{eff} vs. T curves with $J = -34.3\ cm^{-1}$, $J' = -4.7\ cm^{-1}$, $D_i = -0.9\ cm^{-1}$, $g_i = 2.0$ (fixed), $E/D = 0.33$ (fixed) show very good agreement with the experimental data (Figure 3, circles). We recall that the sign of D is physically meaningless with $E/D = 0.33$, as the highest and the lowest Kramers doublets of the sextet are equivalent except for an interchange of coordinate axes.

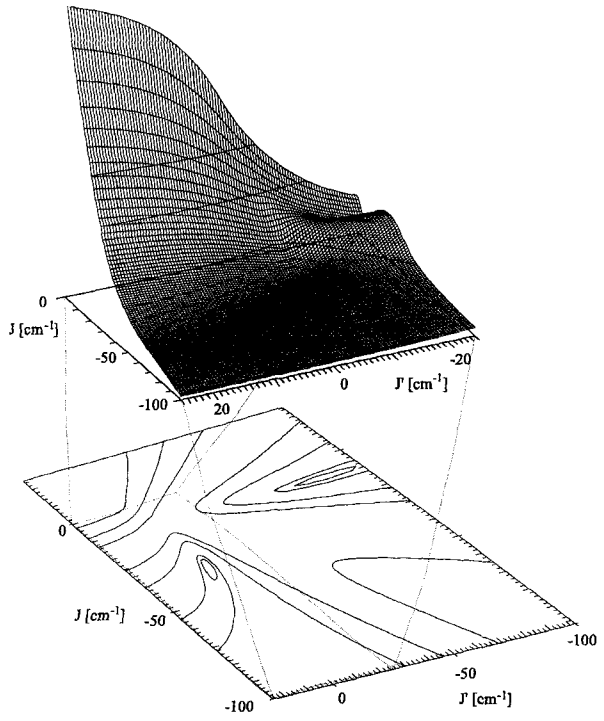

Figure 4. Relative error surface for fitting the variable-temperature magnetic susceptibility data of complex **1**. Only the region of parameter space which gives the smallest relative errors is shown.

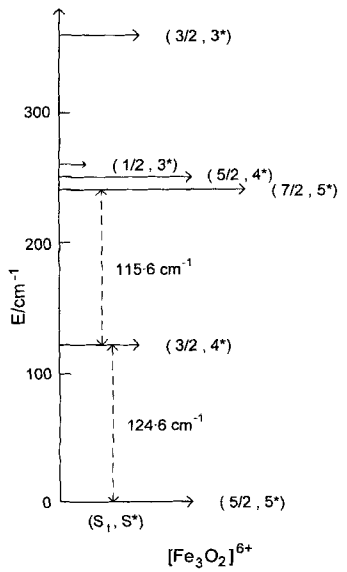

Figure 5. Energy diagram of the low-energy states for complex **1**. The energy of the ground state $S_t = 5/2$ has been set arbitrarily to 0 cm^{-1}. The numbers in parentheses indicate the values of S_t and S^* for each state; $J = -34.3\ cm^{-1}$, $J' = -4.7\ cm^{-1}$.

It is interesting to note the broad minimum in μ_{eff} at $\approx 100-115$ K (Figure 3), a result that can be readily understood if one considers the spin ladder (Figure 5) above the ground state $|S_t = 5/2, S^* = 5\rangle$. From the evaluated exchange coupling constants, the first and second excited states are found to be $|S_t = 3/2, S^* = 4\rangle$ and $|S_t = 7/2, S^* = 5\rangle$, respectively, which lie 124.5 cm^{-1} and 240.1 cm^{-1} above the ground state with $S_t = 5/2$. Since the total spin of the first excited state is 3/2, its population with increasing temperature reduces the effective magnetic moment of **1**. Population of the second excited state with $S_t = 7/2$ occurs above ≈ 115 K, which accounts for the increase in μ_{eff} at higher temperatures. As a result, a minimum is observed in the magnetic moment curve. Finally, it may be noted that the observed ratio J/J' of 7.3 is consistent with the $|S_t = 5/2, S^* = 5\rangle$ ground state predicted in the literature.[14]

The evaluated coupling constant J ($-34.3\ cm^{-1}$) for **1** does fall in the range that has been observed for basic iron carboxylates,[15] lending some credibility to the formulation of **1** as a complex containing the $[Fe_3O]^{7+}$ core. In other words, the μ_2-OPh bridge hardly contributes directly to the exchange coupling between Fe(1) and Fe(2), and the $[Fe_3(\mu_3\text{-}O)(\mu_2\text{-}OPh)]^{6+}$ unit in **1** can be viewed as a triangular Fe_3O^{7+} unit to which has been added a phenoxide moiety, PhO^-. Phenolate bridge formation between Fe(2) and Fe(1) increases the Fe(1)–μ_3-O(1) and Fe(2)–μ_3-O(1) bond lengths and thus diminishes the antiferromagnetic exchange coupling in a manner similar to protonation or metalation of the μ-oxo bridge. Thus the exchange coupling constant $J' = -4.7\ cm^{-1}$ is observed along the short edge of the isosceles triangle. The occurrence of oximate bridges along the edges complicates the situation, however. The problem can be simplified by assuming that the μ_3-oxo atom provides the main superexchange pathway in **1**.

It is pertinent at this point to compare **1** with the related trinuclear complex of 1,1,2-tris(1-methylimidazol-2-yl)ethoxide ($tieo^-$), $[Fe_3O(tieo)_2(O_2CPh)_2Cl_3]$ (**2**),[16] and the dinuclear complex of H_3salmp, $[Fe_2(salmp)_2]$ (**3**).[9] All complexes with an $Fe^{III}_2(O-X)_2$ bridge like that in **1** are antiferromagnetic and show relatively weak spin coupling with values ranging from ≈ -5 to $-20\ cm^{-1}$, with the exception of the dinuclear complex of H_3salmp **3**, which is weakly ferromagnetically coupled, with $J' = +1.21\ cm^{-1}$.[9] These observations extend over more than 20 compounds. The observed J' value for **1** falls at the lower end of the observed range. The evaluated J value for **1**, $-34.3\ cm^{-1}$, is significantly smaller than that in the similar trinuclear complex **2**, for which the equivalent coupling constant is $-55\ cm^{-1}$.[16] The significantly shorter Fe–O bonds in **2** might account for the stronger coupling in **2** in comparison with that in our complex **1**. It must be pointed out that in the limit of weak interactions, the exchange coupling constant is also sensitive to small angular changes or distortions, but to a lesser degree.

Electron paramagnetic resonance: In order to characterize further the electronic structure of the individual Fe^{III} sites in **1** and to probe their contributions to the spin ground state, the macroscopic magnetic measurements of **1** were complemented by X-band EPR and Mössbauer measurements.

The relatively large energy separation of ground-state and excited-state multiplets justifies a simplified spin-Hamiltonian description of the spin ground state according to Equation 2, where $S = S_t$ is the total spin of the spin multiplet and D_t and

$$\mathcal{H} = D_t[S_z^2 - S(S+1)/3 + (E/D_t)(S_x^2 - S_y^2)] + \mu_B \boldsymbol{B} g \boldsymbol{S} \qquad (2)$$

E/D_t are the corresponding axial and rhombic zero-field parameters. Although the approximation is exact only for infinitely strong exchange coupling it is well justified here for interpretation of low-temperature EPR and magnetic Mössbauer spectra, as a closer inspection of the susceptibility calculations in fact revealed negligible mixing of excited and ground state spin multiplets at any applied field, because of relatively small D values.

Resolved EPR spectra could be obtained from **1** at temperatures below approximately 60 K. The spectra measured in acetonitrile solution are dominated by a prominent signal at $g = 4.3$ and an asymmetrical line at $g \approx 9.6$. The pattern is typical of spin $S_t = 5/2$ with "strong" zero-field splitting $|D_{5/2}| > h\nu$ (0.3 cm^{-1} at X-band),[17] in agreement with the susceptibility measurement. From a rhombogram[18] for $S = 5/2$ the signals can be assigned to the isotropic middle Kramers doublet ($g = 4.3$) and the anisotropic lowest or highest doublet ($g \approx 9.6$) of the sextet, revealing a large rhombicity parameter $E/D_{5/2} = 0.3$. This parameter is most accurately detectable from the EPR data. It is hard to measure with high accuracy from other techniques. As the EPR signals originate from different Kramers doublets their intensity ratio yields an estimate for the axial zero-field parameter $D_{5/2}$. For **1** the EPR signal amplitudes and widths appeared to be constant relative to each other, within experimental error, in the temperature range 5–20 K. We concluded that the splitting $3.5 \times |D_{5/2}|$ of ground and middle Kramers doublets must be less than approx. 3.45 cm^{-1} ($= kT$ at 5 K), which means that $|D_{5/2}|$ is of the order of 1 cm^{-1}. To compare this value with that of the susceptibility result $|D_i| = 0.9$ cm^{-1}, one has to convert the local zero-field parameter D_i that is related to individual iron spins $S = 5/2$ into $D_{5/2}$, valid for the total spin $S_t = 5/2$ of the molecule. Using spin projection coefficients[19] for the $|S_t = 5/2, S^* = 5\rangle$ sextet, one obtains $D_{5/2} = 1.59 \times D$ (adopting the previous assumption of identical local D values for the three iron sites). Substitution of the susceptibility result yields $|D_{5/2}| = 1.4$ cm^{-1}, in accordance with the estimate from EPR signals. Further discussions refer to this value.

We finally note that no EPR signals could be obtained from excited spin multiplets at elevated temperatures, presumably because of undetectably broad lines. As the experimental spectra of the ground-state multiplet exhibit increasing broadening at temperatures above about 40 K the supposed reason is that spin relaxation processes are strongly enhanced by the increasing thermal population of excited spin states.

Mössbauer isomer shifts and quadrupole splittings: The zero-field Mössbauer spectrum of solid **1** is an asymmetrical doublet that can be deconvoluted at temperatures above 150 K into two Lorentzian-shaped quadrupole doublets with an area ratio of 1:2. A least-squares fit of the spectrum at 200 K (Figure 6 A) yields isomer shifts $\delta(1) = 0.43$ $mm\,s^{-1}$, $\delta(2) = 0.47$ $mm\,s^{-1}$, and quadrupole splittings $\Delta E_Q(1) = 1.10$ $mm\,s^{-1}$, $\Delta E_Q(2) = 0.64$ $mm\,s^{-1}$ with linewidths $\Gamma(1) = \Gamma(2) = 0.38$ $mm\,s^{-1}$. Linewidths and line depths of this fit were correlated by factors of 1 and 2, respectively. Alternative fit models without constraints or with three independent subspectra did not greatly improve the quality of the simulations and gave fairly arbitrary intensity ratios, and were therefore discarded. On the other hand, the line assignments of the fit presented in Figure 6 A were further corroborated by magnetically perturbed spectra described later.

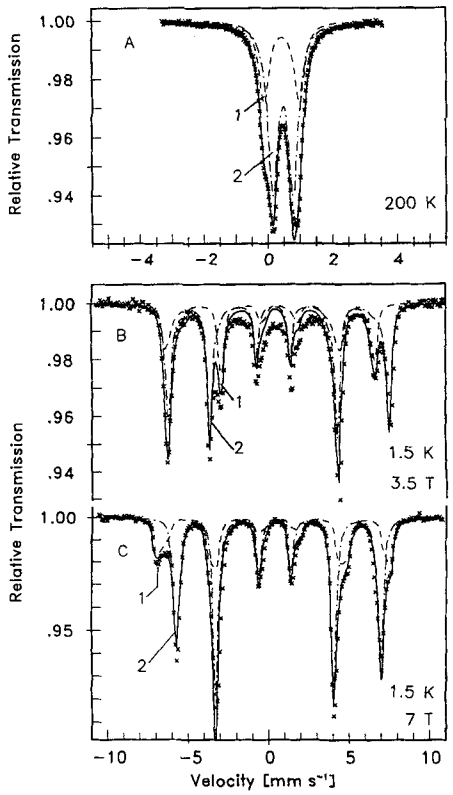

Figure 6. Mössbauer spectra of polycrystalline **1** at 200 K, $B = 0$ (trace A), 1.5 K with $B = 3.5$ T (trace B) and 1.5 K with $B = 7$ T (trace C). The magnetic field applied was perpendicular to the γ-radiation beam. The solid line is the superposition of two subspectra, labeled 1 (- - -) and 2 (— · —), with intensity ratio 1:2. The subspectra are the result of a fit with Lorentzian lines (A) or of a spin-Hamiltonian simulation (B and C), from the values of Table 3.

The subspectra (1) and (2), with an intensity ratio of 1:2, can be unambiguously attributed to the five-coordinated ion Fe(3) (subspectrum (1)) and the two six-coordinated ions Fe(1) and Fe(2) (subspectrum (2)), respectively (compare the molecular structure in Figure 2). The Mössbauer isomer shifts together with the quadrupole splittings support the ferric high-spin state for the three iron sites. The difference in the isomer shifts of Fe(1)/Fe(2) and Fe(3) might be attributed to the shorter bond lengths at the pentacoordinated site Fe(3) and consequently the increased covalency of the bonds. It is interesting to note that the quadrupole splitting of the five-coordinated Fe(3) is unusually large for a high-spin ferric iron and significantly exceeds the value of the six-coordinated sites Fe(1) and Fe(2). It is in the range for Fe^{III} compounds with known or postulated μ_2-oxo bonds.[20] The six-coordinated ferric ions Fe(1) and Fe(2), on the other hand, remain indistinguishable in the Mössbauer spectra under any conditions of temperature or applied magnetic field.

Magnetic Mössbauer spectra: The sign of the main component V_{zz} and the asymmetry parameter η of the electric field gradient tensor (EFG), which yield further information about symmetry

0947-6539/97/0302-0198 $ 15.00+.25/0 Chem. Eur. J. 1997, 3, No. 2

properties of the iron ligand field, were determined from magnetic Mössbauer spectra measured at 1.5 K (Figure 6 B and C). For both iron sites, Fe(1)/Fe(2) as well as Fe(3), we found V_{zz} to be negative and $\eta = 0$ (within error range 0.3). It should be noted that high-field/high-temperature measurements were not as conclusive for the determination of the EFG as they usually are for magnetic monomers. The internal fields do not collapse sufficiently to allow unique line assignments with respect to the applied field. This is due to the significant population of excited magnetic states of the trimer at elevated temperatures. At 130 and 200 K with a 7 T field (not shown) only the outermost magnetic lines of subspectrum (1) were sufficiently resolved. Their positions and intensities, however, again corroborated $V_{zz} < 0$ and $\eta \approx 0$ for the Fe(3) site.

Magnetic hyperfine interactions of the ^{57}Fe nuclei were also measured to probe the partial contributions of the individual ferric ions to the total spin ground state of the trinuclear compound **1**. To this end, magnetically perturbed Mössbauer spectra were measured from polycrystalline samples at and below liquid helium temperatures. Applied fields of 3.5 and 7 T induce well-resolved spectra with overall splitting of $\approx 13\ mm\,s^{-1}$, which implies internal fields $\boldsymbol{B}^{int}$ in excess of 42 T but much less than the 55 T observed in most mononuclear high-spin ferric compounds. Temperature variations showed that the Mössbauer lines are broadened by intermediate spin relaxation rates (on the Mössbauer timescale) even at 4.2 K. Only at the experimental base temperature of 1.5 K are the spectra virtually unaffected by spin relaxation processes, indicating stationary internal fields. At the lowest temperature the relaxation is ineffective because at applied field the lowest electron magnetic sublevel is populated exclusively. On the other hand, temperature elevation to more than 30 K is required to approach the fast relaxation limit where narrow Mössbauer lines are observed again. At the higher temperatures, however, sensitivity for ground-state properties like zero-field splitting becomes low. Therefore, in order to avoid tedious line-shape analyses for broadened Mössbauer relaxation spectra, we focused our analyses on measurements at 1.5 K with fields higher than 3 T.

As shown in Figure 6 (B, C) the magnetic Mössbauer spectra consist of two six-line patterns with an intensity ratio of 1:2, resembling the two subspectra (1) and (2) observed at zero field. This feature is most obvious from the splitting of the outer lines in the 7 T spectrum (trace C, Figure 6). Comparison of traces B and C in Figure 6 shows that variations of the applied field change the two subspectra in different manners. The total splitting of the low-intensity sextet, subspectrum (1), significantly *decreases* when the magnetic field is decreased from 7 to 3.5 T, while the splitting of subspectrum (2) for the same change in field *increases*. This opposite behavior of the two sextets clearly demonstrates the antiparallel alignment of the corresponding iron spins in forming the magnetic ground state $|S_t = 5/2, S^* = 5\rangle$ of the trinuclear molecule. The spins of Fe(1) and Fe(2), which both account for subspectrum (2), are obviously parallel to each other, but antiparallel coupled to the spin of the Fe(3) site with subspectrum (1).

The magnetic Mössbauer subspectra were further characterized by means of the spin Hamiltonian for the total spin $S_t = 5/2$ in the limit of infinitely strong spin coupling [Eq. (2)], as for the EPR interpretations. The ^{57}Fe hyperfine interactions were derived from separate diagonalization of the usual nuclear Hamiltonian[17] and the hyperfine coupling terms $\boldsymbol{S}\cdot\boldsymbol{a}(i)\cdot\boldsymbol{I}(i)$ for total electronic spin $\boldsymbol{S}$ and nuclear spins $\boldsymbol{I}(i)$ of the subspectrum $i = 1,2$ were evaluated with electronic spin expectation values $\langle\boldsymbol{S}\rangle$ replacing $\boldsymbol{S}$. This approach leads to internal fields $\boldsymbol{B}^{int}(i) = \boldsymbol{a}(i)/g_N\beta_N\langle\boldsymbol{S}\rangle$ at the ^{57}Fe nuclei. The strength and orientation of $\boldsymbol{B}^{int}$ in the molecular frame depend through $\langle\boldsymbol{S}\rangle$ on the zero-field parameters as well as on strength and direction of the applied field. The field dependence of the experimental spectra therefore gave the clues in the choice of the spin Hamiltonian and hyperfine parameters. The $\boldsymbol{a}(i)$ tensors for the two subspectra were taken to be colinear and diagonal in the principal axis system of the total spin.

A search in the parameter manifold starting with the output of EPR and magnetic susceptibility for the electronic parameters led to the values listed in Table 3. The simulations for powder-distributed molecules show that the measured magnetic hyperfine splittings and line shapes of the powder spectra at moderate and strong field depicted in Figure 6 B,C are consistent with $|D_{5/2}|$ in the range ≈ 1–$2.5\ cm^{-1}$ for $E/D_{5/2} = 0.33$. As both parameters were partially covariant in the fits, the values $|D_{5/2}| = 1.4\ cm^{-1}$ and $E/D_{5/2} = 0.33$ as derived from the magnetic susceptibility and EPR data were fixed also for the analyses of the hyperfine parameters.

The lowest Kramers doublet of the rhombic $S_t = 5/2$ sextet ($E/D_{5/2} = 0.33$) is magnetically anisotropic (as is reflected by the effective EPR g values) with an easy axis of magnetization in the y or z direction, depending on the sign of $D_{5/2}$. For arbitrarily oriented (weak) fields the spin expectation value is large and preferentially aligned along the easy axis fixed in the molecular frame. The Mössbauer internal fields $\boldsymbol{B}^{int}$ are therefore also fixed in the same molecular direction (adopting the isotropic hyperfine coupling tensor). For powder-distributed molecules this leads to widely split line sextets with relative line intensities close to the ratio 3:2:1:1:2:3, which is the limit for uniform orientation distribution of the effective field relative to the γ-ray beam. The 3.5 T spectrum of **1** in Figure 6 B closely resembles this feature. The stronger field of 7 T (trace C) changes the line intensities towards a ratio 3:4:1:1:4:3, which is the limit for

Table 3. Mössbauer and spin-Hamiltonian parameters of **1**.

Subspectrum [a]	Site	$D_{5/2}$ (cm^{-1}) [b]	$E/D_{5/2}$ [b]	δ ($mm\,s^{-1}$)	ΔE_Q ($mm\,s^{-1}$)	η	α (°) [c]	β [c]	γ [c]	$a/g_N\beta_N$ (T)	$A/g_N\beta_N$ (T)
1	Fe(3)	−1.4	0.33	0.45(1)	−1.10(2)	0(0.3)	90	20	0	+15.0(2)	−21.0
2	Fe(1)/Fe(2)			0.49(1)	−0.63(2)	0(0.3)	90	90	0	−18.6(2)	−21.7

[a] The magnetic Mössbauer spectra are simulated with intrinsic linewidth $\Gamma = 0.3\ mm\,s^{-1}$. [b] Values for the total spin of the ground state $S_t = 5/2$. The corresponding local values used in the simulation of the susceptibility data are $D_i = 0.9\ cm^{-1}$, $E/D_i = 0.33$. [c] Euler angles for rotation of the principal axes of the zero-field interaction into those of the EFG_1 sequence $R(\alpha,z) \rightarrow R(\beta,y') \rightarrow R(\gamma,z'')$.

alignment of $\boldsymbol{B}^{int}$ along the applied field perpendicular to the γ-rays. This means that the strong external field perturbs the electronic levels considerably and forces the spin expectation values out of the molecular easy axis. The Mössbauer hyperfine fields $\boldsymbol{B}^{int}(i)$ in the powder sample therefore tend to sense all components of the coupling tensors $\boldsymbol{a}(i)$, while in the first case of moderate applied field mainly the $\boldsymbol{a}(i)$ components along the easy magnetic axis are effective. The simulations of the measured spectra Figure 6 B,C for the different experimental conditions showed that any magnetic anisotropy detectable in the Mössbauer spectra can be explained by the properties of the electronic spin system; no indications were found for additional $\boldsymbol{a}(i)$ anisotropy (within an estimated error range of 0.5 T for the possible differences of the $\boldsymbol{a}$ components). The resulting isotropic coupling constants in the two subspectra (1) and (2) were $a(1)/g_N\beta_N = +15.0$ T and $a(2)/g_N\beta_N = -18.6$ T. We recall that the values express the ^{57}Fe hyperfine splittings in terms of the total spin $\boldsymbol{S}_t$ rather than the local spins $\boldsymbol{S}_i$, and the opposite signs of $a(1)$ and $a(2)$ again reflect the antiparallel coupling of the respective iron spins. The intrinsic A values in the system of the individual spins $S_i = 5/2$ ($i = 1,2,3$) can be derived from spin projections of the S_i on the total spin state $|S_t = 5/2, S^* = 5\rangle$.[19] Amazingly, the Mössbauer data permitted identification of the iron sites Fe(1) and Fe(2) with S_1 and S_2 forming the intermediate spin $S^* = 5$ and the antiparallel coupled site Fe(3) with S_3. For negligible mixing of spin multiplets the following relations hold: $\langle M'|\boldsymbol{S}_1|M\rangle = 6/7\langle M'|\boldsymbol{S}_t|M\rangle$, $\langle M'|\boldsymbol{S}_2|M\rangle = 6/7\langle M'|\boldsymbol{S}_t|M\rangle$, $\langle M'|\boldsymbol{S}_3|M\rangle = -5/7\langle M'|\boldsymbol{S}_t|M\rangle$, where the matrix elements are taken in the ground state multiplet. From the equivalence of the hyperfine term $\boldsymbol{S}_t \cdot a(i) \cdot \boldsymbol{I}(i)$ with the intrinsic form $\boldsymbol{S}_j \cdot A_{Fe(j)} \cdot \boldsymbol{I}_j$ for individual electron spin $\boldsymbol{S}_j$, one obtains for Fe(3) from subspectrum (1) $A_{Fe(3)} = -7/5\,a(1)$, while for the equivalent sites Fe(1) and Fe(2) from subspectrum (2), the relation is $A_{Fe(1)/Fe(2)} = +7/6\,a(2)$. Substitution of the results from above yields $A_{Fe(3)}/g_N\beta_N = -21.0$ T and $A_{Fe(1)/Fe(2)}/g_N\beta_N = -21.7$ T, which is in agreement with what is expected for high-spin ferric iron with weak O and N ligands. Since the intrinsic hyperfine constants $A_{Fe(j)}/g_N\beta_N$ of the high-spin ferric iron arise primarily from the Fermi contact term, it is expected to be isotropic and close to 22 T. One might speculate that the small reduction for the five-coordinated site Fe(3) with respect to the six-coordinated sites owes its origin to the slightly shorter bonds around Fe(3) and the corresponding increase in covalency. It might be significant, as the same tendency was found for the isomer shifts.

The quadrupole line shifts in the magnetic Mössbauer spectra of **1** reveal effective quadrupole splittings; for subspectrum (1), these are virtually equal to $\Delta E_Q(1)$ of the zero-field spectrum, but for subspectrum (2) they correspond to only about $\frac{1}{2} \times \Delta E_Q(2)$ at zero field. The apparent signs of the splittings are opposite for the two subspectra, positive for subspectrum (1) but negative for (2). For strong internal fields, as in the case of compound **1**, the effect of quadrupole interaction in the spectra is determined in the first order by the component of the EFG along $\boldsymbol{B}^{int}$. Provided the asymmetry parameter is zero, this means that EFG(1) is oriented with its main component V_{zz} essentially parallel to $\boldsymbol{B}^{int}$, but V_{zz} of EFG(2) is perpendicular to $\boldsymbol{B}^{int}$ and the magnetic Mössbauer spectrum senses an EFG component close to the V_{xx}/V_{yy} plane. Systematic trials were performed to determine quantitative values for the asymmetry parameters and the Euler angles of the EFGs in the coordinated system of the total spin. For the sake of simplicity only tensor rotations were regarded with no more than one Euler angle differing from 0 or 90°. The best results from the simulations are given in Table 3. For simplicity of the coordinate system we selected $D<0$ to have the electronic spin expectation value and the internal fields $\boldsymbol{B}^{int}$ in the z direction. The relative orientation of the EFG tensors and $\boldsymbol{B}^{int}$ for this choice is sketched in Scheme 3. We notice that the two contributions from Fe(1) and Fe(2) to EFG(2), subspectrum (2), appear to be identical.

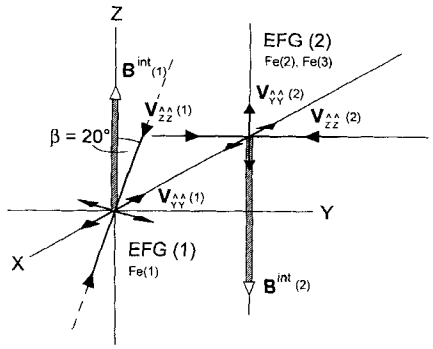

Scheme 3. The relative orientation of the EFG tensors and $\boldsymbol{B}^{int}$ for $D<0$.

The accuracy, however, is not very high and we cannot finally exclude some angle between the EFG tensor axes, provided $\boldsymbol{B}^{int}$ remains perpendicular to V_{zz}. Rotations of the EFG around the final z axis are meaningless anyway, as $\eta \approx 0$. The correlations of the EFG tensors with the molecular coordination polyhedra of the ferric ions in **1** are not obvious for the rather "irregular" octahedral sites Fe(1) and Fe(2) and cannot be predicted without detailed calculations. In contrast, for the quasi-trigonal bipyramidal site Fe(3) from symmetry arguments the main component V_{zz} of the EFG should lie along the "axis" O(1)-Fe(3)-O(31) to be consistent with $\eta(1) \approx 0$. It is interesting to note that the tilting angle $\theta = 16°$ of the O(1)–Fe(3) bond out of the Fe plane from the X-ray structure closely resembles the Euler angle $\beta = 20°$ between $V_{zz}(1)$ and $\boldsymbol{B}^{int}$; one is tempted to assume that $\boldsymbol{B}^{int}$ is in the Fe(1)-Fe(2)-Fe(3) plane. Since for high-spin Fe^{III} the EFG and the local zero-field interactions can be expected to exhibit identical principal axes and usually have the same symmetry properties, according to the relation $E/D \approx {}^1/_3\eta$, one may conclude that the observed rhombicity of the total spin ground state does not necessarily originate from local rhombicity but is the result of tensorial superpositions of local axial interactions in rotated coordinate systems.

Both the three-iron cluster of **1** and that of site 3 in ferreascidin have $S = 5/2$ with two Fe^{III} ions, which are indistinguishable by means of their Mössbauer spectra, spin-aligned parallel and coupled antiparallel to the third Fe^{III}. The Mössbauer isomer shifts of the Fe^{III} ions Fe(1)/Fe(2) in **1** (0.49 mm s^{-1}) are furthermore identical to that of Fe^{III} from site 3 in ferreascidin (0.5 mm s^{-1}, average value given in ref. [6]). The same holds for the quadrupole splittings in the magnetic Mössbauer spectra; ≈ 0.62 mm s^{-1} for Fe(1)/Fe(2) in **1** and ≈ 0 mm s^{-1} for site 3 of ferreascidin. The values are typical of ferric high-spin ions in

0947-6539/97/0302-0200 $ 15.00+.25/0 Chem. Eur. J. 1997, 3, No. 2

five- or six-coordination with O- and N-ligands. Remarkable differences, however, can be seen for the third Fe^{III} ion of the model cluster **1**. Whereas in the protein the third Fe^{III} is only distinguishable from its neighbors by the opposite orientation of its Mössbauer hyperfine field, the corresponding third Fe^{III} in **1** has a distinctly larger quadrupole splitting and lower isomer shift. If we can relate the Mössbauer parameters of Fe(3) to the "short" (μ_3-O) bond in **1**, this discounts such a bond for the trimeric site 3 in ferreascidin.

The basic analysis of the magnetic Mössbauer spectra of ferreascidin in ref. [6] is not easy to compare with the full spin-Hamiltonian analysis that was possible for the synthetic model complex **1**, as the first does not parameterize the magnetic anisotropy of the cluster using zero-field and hyperfine coupling parameters and appropriate powder average. The difference in the internal hyperfine field, $\boldsymbol{B}^{int}$, given for the antiparallel-coupled ferric ions in the ferreascidin cluster at the strongest applied field (11.1 T), however, can be used for a comparison. The value 7.6 T[6] is close to what we expect for the difference of the saturation values of the internal fields, $\boldsymbol{B}^{sat} = |a|/g_N\beta_N$ 5/2. From the spin-Hamiltonian parameters for **1** (Table 3) we obtain $\boldsymbol{B}^{sat} = 37.5$ and 46.4 T for Fe(3) and Fe(1)/Fe(2), respectively, which means a maximum difference of 9 T. One can take the correspondence to the values for ferreascidin as an indication of identical spin projection factors for the different iron sites in the two trimeric clusters, that is, in fact both the model cluster and the protein cluster exhibit the same type of spin ground state ($S_t = 5/2$, $S^* = 5$).

To conclude, a trinuclear iron(III) cluster **1** containing an isosceles triangular arrangement of the ferric ions has been assembled with bridging oxo and phenoxo groups; **1** is a potential candidate as a structural model for the iron-binding site 3 in ferreascidin, as it shares many, but not all, of the characteristics of site 3.

Acknowledgement: This work was initiated at the Ruhr-Universität Bochum. Our thanks are due to Prof. K. Wieghardt for his generous help and interest. The technical assistance of M. Hess is greatly appreciated.

Received: August 29, 1996 [F451]

[1] See for example: a) A. L. Feig, S. J. Lippard, *Chem. Rev.* **1994**, *94*, 759; b) D. M. Kurtz, *ibid.* **1990**, *90*, 585; c) L. Que, A. E. True, *Prog. Inorg. Chem.* **1990**, *38*, 98; d) J. B. Vincent, G. L. Olivier-Lilley, B. A. Averill, *Chem. Rev.* **1990**, *90*, 1447.

[2] a) A. Caneschi, A. Cornia, S. J. Lippard, G. C. Papaefthymiou, R. Sessoli, *Inorg. Chim. Acta* **1996**, *243*, 295; b) A. Caneschi, A. Cornia, A. C. Fabretti, D. Gatteschi, *Angew. Chem.* **1995**, *107*, 2862; *Angew. Chem. Int. Ed. Engl.* **1995**, *34*, 2716; c) S. Parsons, G. A. Solan, R. E. P. Winpenny, *J. Chem. Soc. Chem. Commun.* **1995**, 1987; d) K. L. Taft, G. C. Papaefthymiou, S. J. Lippard, *Science* **1993**, *259*, 1302; e) K. L. Taft, C. D. Delfs, G. C. Papaefthymiou, S. Foner, D. Gatteschi, S. J. Lippard, *J. Am. Chem. Soc.* **1994**, *116*, 823; f) A. K. Powell, S. L. Heath, D. Gatteschi, L. Pardi, R. Sessoli, G. Spina, F. Del Giallo, F. Pieralli, *ibid.* **1995**, *117*, 2491; g) W. Micklitz, V. McKee, R. L. Rardin, L. E. Pence, G. C. Papaefthymiou, S. G. Bott, S. J. Lippard, *ibid.* **1994**, *116*, 8061; h) M. Mikuriya, Y. Hashimoto, S. Nakashima, *J. Chem. Soc. Chem. Commun.* **1995**, 295; i) C. D. Delfs, D. Gatteschi, L. Pardi, R. Sessoli, K. Wieghardt, D. Hanke, *Inorg. Chem.* **1993**, *32*, 3099; j) J. K. McCusker, C. A. Christmas, P. M. Hagen, R. K. Chadha, D. F. Harvey, D. N. Hendrickson, *J. Am. Chem. Soc.* **1991**, *113*, 6114; k) V. S. Nair, K. S. Hagen, *Inorg. Chem.* **1992**, *31*, 4048.

[3] a) A. I. Vogel, *Macro and Semimicro Qualitative Analysis*, Longmans, London, **1973**; b) B. McCudden, *J. Chem. Soc. Dalton Trans.* **1983**, 2043.

[4] a) J. Grigg, D. Collison, C. D. Garner, M. Helliwell, P. A. Tasker, J. M. Thorpe, *J. Chem. Soc. Chem. Commun.* **1993**, 1807; b) V. Zerbib, F. Robert, P. Gouzerh, *ibid.* **1994**, 2179; c) V. Y. Kukushkin, V. K. Belsky, E. A. Aleksandrova, V. E. Konovalov, G. A. Kirakosyan, *Inorg. Chem.* **1992**, *31*, 3836.

[5] L. C. Dorsett, C. J. Howkins, J. A. Grice, M. F. Lavin, P. M. Merefield, D. L. Parry, I. L. Ross, *Biochemistry* **1987**, *26*, 8078.

[6] S. W. Taylor, J. D. Cashion, L. J. Brown, C. J. Hawkins, G. R. Hanson, *Inorg. Chem.* **1995**, *34*, 1487.

[7] S. Slappendel, G. A. Veldink, J. F. G. Vliegenhardt, R. Aasa, B. Malmström, *Biochem. Biophys. Acta* **1980**, *642*, 30.

[8] G. A. Olah, M. Arvanaghi, G. K. Surya Prakash, *Synthesis* **1980**, 220.

[9] B. S. Snyder, G. S. Patterson, A. J. Abrahamson, R. H. Holm, *J. Am. Chem. Soc.* **1989**, *111*, 5214.

[10] F. A. Cotton, G. Wilkinson, *Advanced Inorganic Chemistry*, 5th ed., Wiley, New York, **1988**.

[11] a) P. Chaudhuri, M. Winter, P. Fleischhauer, W. Haase, U. Flörke, H.-J. Haupt, *J. Chem. Soc. Chem. Commun.* **1993**, 566; b) P. Chaudhuri, M. Winter, P. Fleischhauer, W. Haase, U. Flörke, H.-J. Haupt, *Inorg. Chim. Acta* **1993**, *212*, 241.

[12] a) R. V. Thundathil, E. M. Holt, S. L. Holt, K. J. Watson, *J. Am. Chem. Soc.* **1977**, *99*, 1818; b) A. B. Blake, L. R. Fraser, *J. Chem. Soc. Dalton Trans.* **1975**, 193; c) W. H. Armstrong, M. E. Roth, S. J. Lippard, *J. Am. Chem. Soc.* **1987**, *109*, 6318.

[13] P. Chaudhuri, M. Winter, unpublished results.

[14] J.-J. Girerd, G. C. Papaefthymiou, A. D. Watson, E. Garup, K. S. Hagen, N. Edelstein, R. B. Frankel, R. H. Holm, *J. Am. Chem. Soc.* **1984**, *106*, 5941.

[15] R. D. Cannon, R. P. White, *Progr. Inorg. Chem.* **1988**, *36*, 195.

[16] S. M. Gorun, G. C. Papaefthymiou, R. B. Frankel, S. J. Lippard, *J. Am. Chem. Soc.* **1987**, *109*, 4244.

[17] A. X. Trautwein, E. Bill, E. L. Bominaar, H. Winkler, *Struct. Bond.* **1991**, *78*, 1.

[18] H. H. Wickman, M. P. Klein, D. A. Shirley, *J. Chem. Phys.* **1965**, *42*, 2113.

[19] A. Bencini, D. Gatteschi, *EPR of Exchange Coupled Systems*, Springer, Berlin, **1990**.

[20] a) J. T. Sage, Y.-M. Xia, P. G. Debrunner, D. T. Keough, J. de Jersey, B. Zerner, *J. Am. Chem. Soc.* **1989**, *111*, 7239; b) P. G. Debrunner in *Biological Magnetic Resonance, Vol. 13* (Eds.: L. J. Berliner, J. Reuben), Plenum, **1993**, p. 59, and references cited therein.